ACS APPLIED MATERIALS & INTERFACES

Research Article

www.acsami.org

# Why Superhydrophobicity Is Crucial for a Water-Jumping Microrobot? Experimental and Theoretical Investigations

Jie Zhao,[†,‡] Xinbin Zhang,[†] Ning Chen,[‡,§] and Qinmin Pan*[,†,§]

[†]State Key Laboratory of Robotics and Systems and [§]School of Chemical Engineering and Technology, Harbin Institute of Technology, Harbin 150001, People's Republic of China

Supporting Information

**ABSTRACT:** This study reported for the first time a novel microrobot that could continuously jump on the water surface without sinking, imitating the excellent aquatic locomotive behaviors of a water strider. The robot consisted of three supporting legs and two actuating legs made from superhydrophobic nickel foam and a driving system that included a miniature direct-current motor and a reduction gear unit. In spite of weighing 11 g, the microrobot jumped 14 cm high and 35 cm long at each leap. In order to better understand the jumping mechanism on the water surface, the variation of forces exerted on the supporting legs was carefully analyzed and calculated based on numerical models and computational simulations. Results demonstrated that superhydrophobicity was crucial for increasing the upward force of the supporting legs and reducing the energy consumption in the process of jumping. Although bionic microrobots mimicking the horizontal skating motions of aquatic insects have been fabricated in the past years, few studies reported a miniature robot capable of continuously jumping on the water surface as agile as a real water strider. Therefore, the present finding not only offers a possibility for vividly imitating and better understanding the amazing water-jumping capability of aquatic insects but also extends the application of porous and superhydrophobic materials to advanced robotic systems.

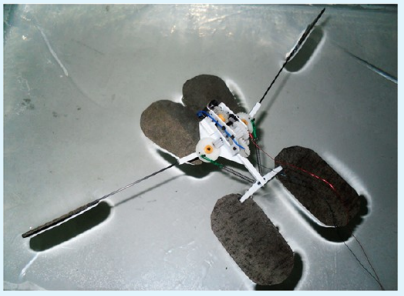

**KEYWORDS:** *water-jumping microrobot, bioinspired, mechanism, numerical model, superhydrophobicity*

## INTRODUCTION

Walking on water may be a dream for human beings, but it has become a step closer for bioinspired microrobots.[1] In the past decade, there has been considerable interest in designing and fabricating insect-inspired miniature robots with unique locomotive abilities. Microrobots mimicking the amazing water-walking abilities of a water strider, a kind of long-legged insect that stands effortlessly and even scoots across the surface of ponds, lakes, and other waterways, were developed with the aim of monitoring water pollution and water supplies and conducting surveillance missions.[2−12]

Sitti et al. first assembled a piezoelectrically driven microrobot with optimized supporting legs, taking inspiration from the water strider and advantage of the surface tension of water.[3] The fabricated robot linearly moved on the water surface at a speed of 3 cm $s^{-1}$ without sinking, providing an alternative route for developing smart and advanced microrobotic systems. Nevertheless, the limited upward force of the supporting legs impeded improvement in the walking speed, agility, and further functionalizations of the robot. Recent studies revealed that the micro- and nanometer binary structures on the legs of a water strider enable the insect to skim across water without sinking.[13−16] Inspired by these findings, Zhang et al.[6] developed a water-walking microrobot supported by 10 superhydrophobic legs and propelled by spirallike actuating legs connected to two miniature motors. Although it weighed as much as 390 water striders, the 15-cm-long microrobot could stand, walk, and turn freely on water, reaching a linear speed of up to 15 cm $s^{-1}$.

While water-walking microrobots[3,6,17−20] were fabricated in the past years to mimic the horizontal skating motions of aquatic insects, until now no study assembled a microrobot agile enough to continuously jump on water like a real water strider. From the viewpoint of technology, a water-jumping microrobot has many advantages over water-walking counterparts because it is more agile and possesses higher obstacle-avoidance capability. However, it remains a big challenge for jumping on water because the legs of an aquatic microrobot are not supported by the rigid surface and they experience surface tension, drag force, hydrostatic force, and inertia.[1] For the microrobot jumping on the water surface, its legs will penetrate into water rather than lift the body upward if they press the water surface with too great force.[7,21] Therefore, the legs of a water-jumping microrobot should move with a force that is sufficiently large to lift the body upward but small enough to avoid sinking themselves, indicating the importance of robot design and the availability of novel materials for legs.

In this study, a novel microrobot capable of continuously jumping on the water surface was assembled to mimic the striking locomotive ability of a water strider. The robot consisted of three supporting legs and two actuating legs in order to increase its motion stability and agility. Considering the large drag force and huge impact exerted on the legs of the

Received: May 7, 2012
Accepted: June 24, 2012
Published: June 25, 2012



  

**Scheme 1. Structural Illustrations for the Microrobot Fabricated in This Study**

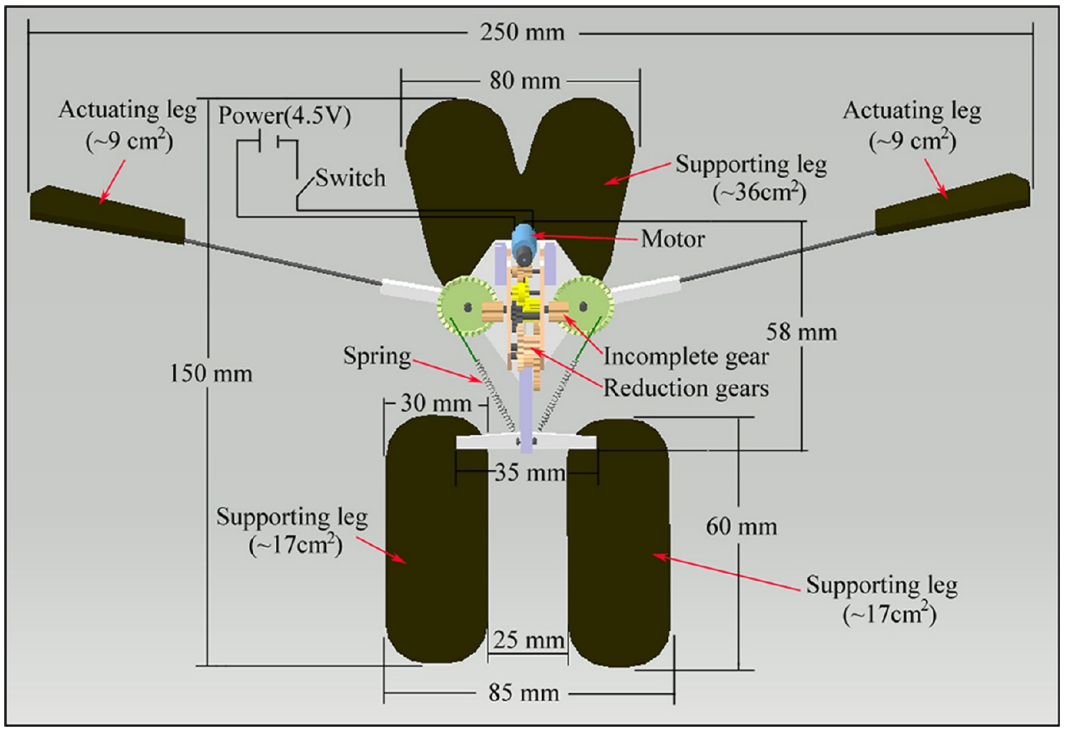


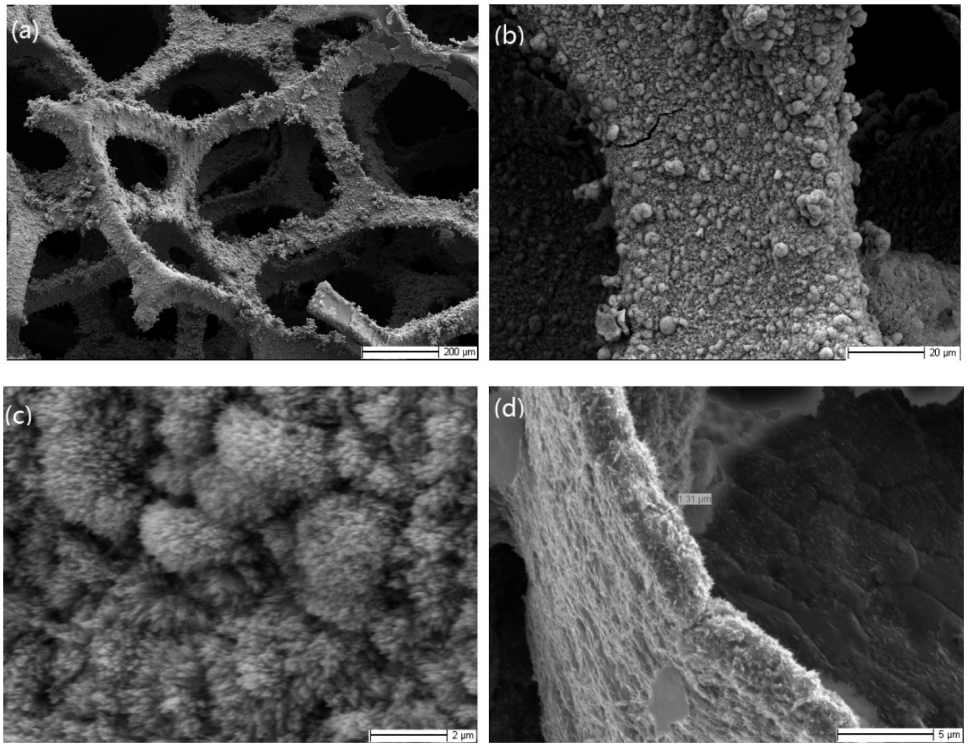


**Figure 1.** (a–c) SEM images of the as-prepared superhydrophobic nickel foam. (d) Cross-sectional image of superhydrophobic nickel foam.

water-jumping robot in the process of jumping and falling,[1,7,21] porous and superhydrophobic nickel foam was used to fabricate the supporting and actuating legs. A miniature direct-current (dc) motor and a reduction gear unit constituted the driving system of the microrobot, which generated an instant force for jumping. Despite the fac that the microrobot weighed more than 1100 water striders, it was still able to continuously jump on the water surface with a maximum height of 14 cm. Numerical models were established to fully understand the jumping mechanism on water. Experimental results and theoretical analyses demonstrated that the superhydrophobicity of the supporting legs was crucial for the robot's jumping capability on the water surface. The present microrobot incorporates improvements over previous counterparts because


dx.doi.org/10.1021/am300794z | ACS Appl. Mater. Interfaces 2012, 4, 3706–3711

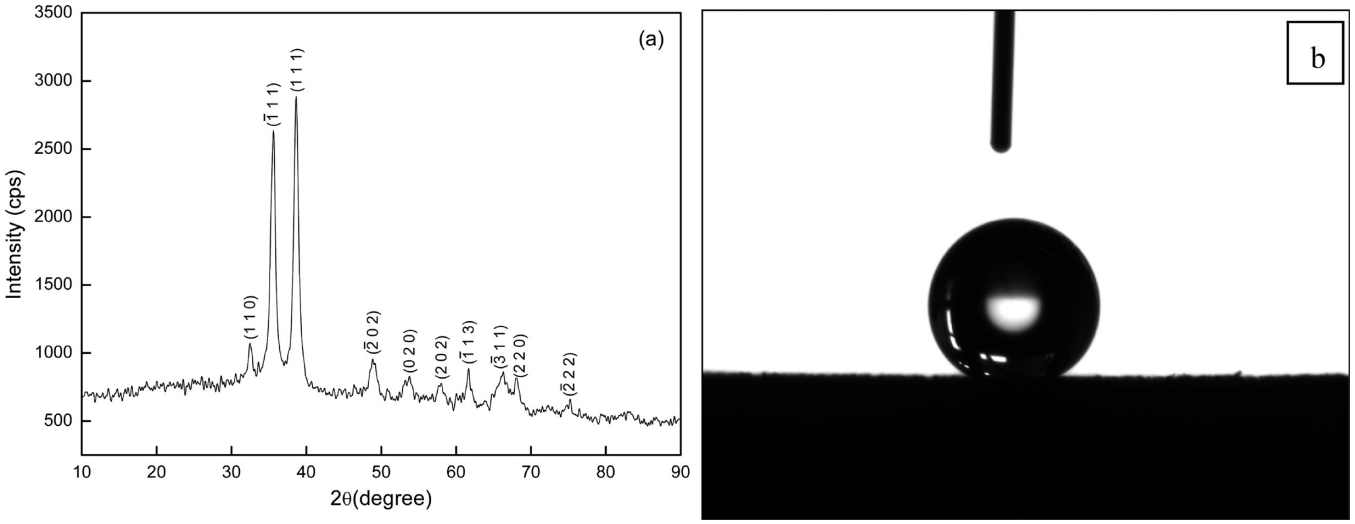


**Figure 2.** XRD pattern (a) and CA measurement (b) of the as-prepared nickel foam.

it is sufficiently agile to continuously jump on water like a water strider, which offers the possibility of vividly mimicking and better understanding the unique locomotive ability of aquatic insects.

## EXPERIMENTAL SECTION

The preparation of superhydrophobic nickel foam was conducted as follows. At first, nickel foam sheets (10 cm × 10 cm × 0.16 cm) were washed with a 5 wt % HCl aqueous solution and distilled water successively. Then the sheets were immersed in 200 mL of ammonia (25%) containing 5−30 mM $Cu_2(OH)_2CO_3$ (basic copper carbonate) at 85−95 °C for 20−30 min. After reaction, black nickel foam sheets were washed with distilled water and dried. The resulting nickel foam sheets were treated with a 10 mM ethanol solution of *n*-dodecanoic acid ($n$-$C_{11}H_{23}COOH$) for 15−30 min. The chemical reactions involved in the above processes are described as follows:

$$Cu_2(OH)_2CO_3 + 2NH_4OH \rightarrow 2CuO + (NH_4)_2CO_3 + 2H_2O \quad (1)$$

$$CuO + 2n\text{-}C_{11}H_{23}COOH \rightarrow Cu(COOC_{11}H_{23})_2 + H_2O \quad (2)$$

Morphologies of the nickel foam sheets were investigated by scanning electron microscopy (SEM; FEI Sirion 200). The contact angles (CAs) of the nickel foam sheets were measured at room temperature (OCA20, DataPhysics Instruments GmbH, Filderstadt) using 4 μL of distilled water as an indicator. X-ray diffraction (XRD) analysis was performed on a Shimadzu XRD-6000. The supporting force of the original and superhydrophobic nickel foam sheets was measured by a DCAT-21 tensiometer (DataPhysics Instruments GmbH, Filderstadt).

The assembly of the water-jumping microrobot was carried out according to the illustration in Scheme 1. The robot consists of three supporting legs, two actuating legs, a miniature dc motor, and a set of plastic reduction gears. The supporting legs are made of superhydrophobic nickel foam sheets. Each actuating leg (12 cm in length) is composed of an incomplete gear, a spring, a carbon fiber bar, and a superhydrophobic nickel foam sheet (~9 $cm^2$) at its end. The incomplete gear is used to latch and release the actuating leg, and the spring is employed to store and release the energy needed for jumping. The actuating legs are connected to the dc motor (0.5 W and 4.5 V) through a set of plastic reduction gears that can reduce the rotation speed and increase the driving torque. There are altogether 11 plastic gears that constitute the reduction mechanism with a speed ratio of 1:13483. Once the operation starts, the dc motor drives the actuating legs to swing forward through the plastic reduction gears. Then the actuating legs are released and swing backward as the incomplete gears rotate to a given angle, generating an instant driving force for jumping. The power supply for the dc motor is sent via two external wires and controlled by a switch.

## RESULTS AND DISCUSSION

**1. Characterizations of Superhydrophobic Nickel Foam.** Figure 1 shows the SEM images of the as-prepared superhydrophobic nickel foam. There are flowerlike clusters coated on the surfaces of the foam skeleton, with an average diameter of ~3 μm. Each cluster is built from nanosheets of a few hundred nanometers in thickness, indicating the presence of binary structures at both micrometer and nanometer scales. The XRD pattern (Figure 2) shows that the chemical compositions of these clusters are mainly cubic CuO. Therefore, flowerlike nanostructured CuO films were coated on the surface of nickel foam through a simple solution-immersion process. The thickness of the CuO coating on the nickel foam is about 1.3 μm (Figure 1d). We also revealed that flowerlike CuO clusters could be deposited on the surface of the nickel foam sheets as the concentration of basic copper carbonate ranged from 5 to 30 mM (see the Supporting Information, Figure S1), indicating little dependence of the morphology on the $Cu_2(OH)_2CO_3$ concentration.

Then water CA measurement was conducted to investigate the wettability of the as-prepared nickel foam sheets. The nickel foam sheets exhibit a water CA of 161°. The sliding angles of the nickel foam sheets were measured as 3.8°. In addition, the as-prepared nickel foam sheets floated on the water surface when contacted with water, forming a dramatic contrast to the original nickel foam sheets. The unsinkable property is believed to arise from the air film surrounding the outer surface of superhydrophobic nickel foam, as illustrated previously.[22] In addition, the superhydrophobic coating on the nickel foam shows desirable mechanical stability. After being cut by scissors, the fracture surface of the nickel foam is still covered with CuO coating, and only a few cracks are observed from the cross-sectional SEM image (see the Supporting Information, Figure S2).

**2. Jumping Behavior of the Microrobot.** The microrobot fabricated in this study is 15 cm long and weights 11 g, which is much larger and heavier than a real water strider (ca. 1.5 cm and 10 mg, respectively). However, it can stand effortlessly on the water surface with three supporting legs

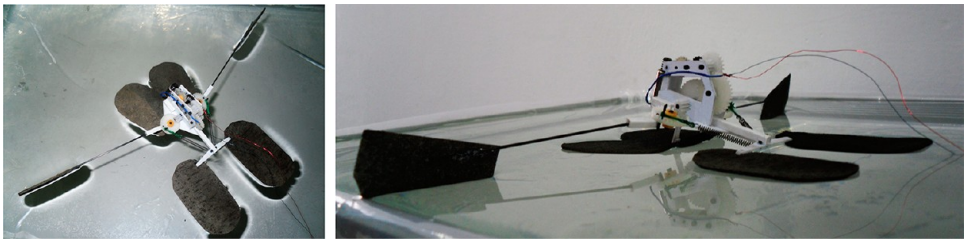

**Figure 3.** Photographs of the water-jumping microrobot standing on the water surface.

(Figure 3). More interesting, the robot is able to continuously jump on the water surface without sinking. Before jumping, two actuating legs are latched by the incomplete gears swung forward at a speed of 30° $s^{-1}$, and the springs are gradually stretched at the same time. Once the incomplete gears rotate 90°, the actuating legs are released and fast swing backward because of the tension of the springs. The superhydrophobic nickel foam sheets at the end of the actuating legs acquire an instant force mainly produced by the hydrodynamic pressure, enabling the robot to leave the water surface at a speed of 1.6 m $s^{-1}$. It can jump 14 cm high and 35 cm long at each leap with a jumping angle ($\beta$) of 20° (see the Supporting Information, movie). The jumping performance of the robot is affected by the jumping angle, as illustrated in Figure 4. The maximum

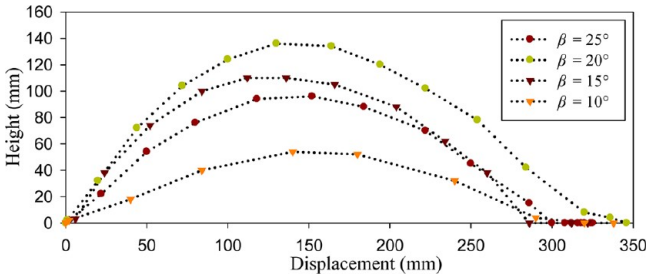


**Figure 4.** Tracks of the microrobot jumping on water with different jumping angles ($\beta$).

jumping height increases along with the jumping angle. Notably, the robot jumps lower at $\beta$ = 25° than at $\beta$ = 20°, which indicates that it is possible that the robot has to overcome a larger drag force with high jumping angle.

**3. Interaction between the Supporting Legs and Water.** The forces exerted on the supporting legs are important factors for the robot's ability to jump on the water surface. Although the interaction between the supporting legs and water is complicated and changeable, a simplified numerical model is established in Scheme 2 to describe the process of a supporting leg leaving or falling on the water surface. The forces exerted on the supporting legs include surface tension ($F_\sigma$) and hydrostatic pressure ($F_s$) that is equal to the weight of displaced water.[1,7] In addition, the supporting legs will suffer from hydrodynamic pressure ($F_d$) and viscous force ($F_v$) once they move on water at a certain speed.[1,7,23−26] Considering that the Reynolds number ($Re$) is much greater than 1 in the jumping process (see the Supporting Information, Table S1), the viscous force ($F_v$) is negligible compared with the hydrodynamic pressure ($F_d$). Then the total force ($F$) exerted on a supporting leg can be described by eq 1,

$$F = F_\sigma \sin\phi + F_s + F_d \tag{1}$$

where $\varphi$ is the angle of the air−water interface at the three-phase contact line. Supposing that a supporting leg (with thickness $\delta$, surface area $S$, perimeter $L$, and contact angle $\theta$) falls or leaves the water surface at a speed of $v$, the $F_\sigma$, $F_s$, and $F_d$ can be written as

$$F_\sigma = \gamma L$$

$$F_s = -\rho g h S$$

$$F_d = -\frac{1}{2} S \rho v |v|$$

where $\gamma$ is the surface tension coefficient of water, $\rho$ is the density difference between water and air, $g$ is the gravitational constant, and $h$ is the height from the supporting leg's bottom to the water surface, respectively. Then eq 1 is written as

$$F = \gamma L \sin\phi - \rho g h S - \frac{1}{2} S \rho v |v| \tag{2}$$

According to the mathematical model of the air−water interface,[5,6]

$$\phi = -2 \arcsin \frac{h_0}{2\sqrt{k}} \tag{3}$$

**Scheme 2. Cross-Sectional Model Describing the Air−Water Interface of a Supporting Leg (a) Leaving and (b) Falling on the Water Surface**

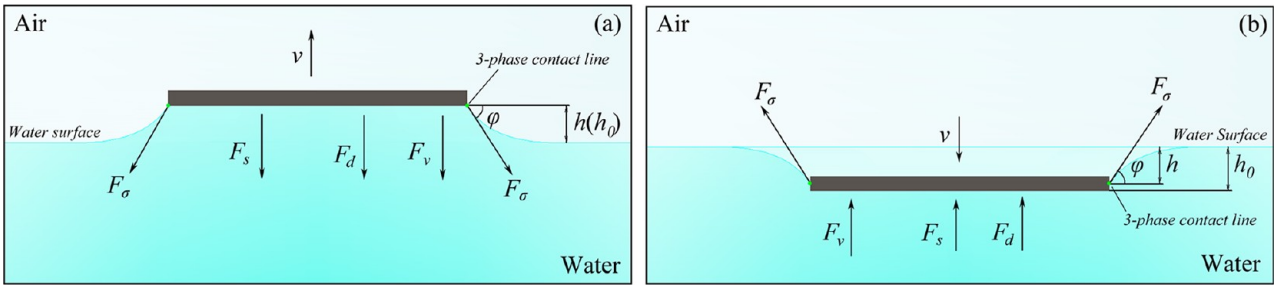

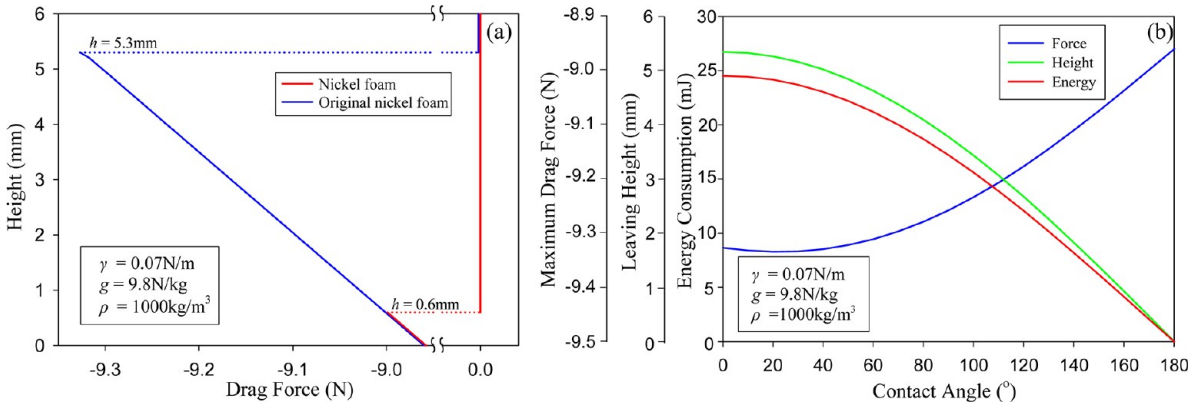


**Figure 5.** (a) Change of the drag force exerted on the supporting legs and original nickel foam sheets with the same size in the process of jumping and (b) influence of the CA on the maximum drag force, leaving height, and energy consumption.

where $k = \gamma/\rho g$ and $h_0$ is the height from the three-phase contact line to the water surface. Here, we assume that the contact angle ($\theta$) is a constant and let $h_\theta$, $h_{\theta-90}$, and $h_{\theta-180}$ equal $h_0$ when $\varphi = \theta$, $\theta - 90°$, and $\theta - 180°$, respectively,

$$\begin{cases} h_\theta = -2\sqrt{k}\,\sin\dfrac{\theta}{2} \\ h_{\theta-90} = -2\sqrt{k}\,\sin\dfrac{\theta-90}{2} \\ h_{\theta-180} = -2\sqrt{k}\,\sin\dfrac{\theta-180}{2} \end{cases}$$

then

$$h_0 = \begin{cases} h,\ h_{\theta-90} \le h \le h_{\theta-180} \\ h_{\theta-90},\ h_{\theta-90} - \delta \le h < h_{\theta-90} \\ h + \delta,\ h_\theta \le h < h_{\theta-90} - \delta \end{cases}$$

According to eq 2, the interaction between the supporting legs and the water surface in the process of jumping and falling can be investigated independently.

**4. Numerical Analysis on the Jumping Process.** Generally, the microrobot has to overcome its own weight and drag force exerted on the supporting legs when it leaves the water surface.[1] As described in Scheme 2a, the drag force consists of surface tension ($F_\sigma$), hydrostatic pressure ($F_s$), hydrodynamic pressure ($F_d$), and viscous force ($F_v$), which can be calculated by eq 2. Figure 5a displays the variation of the drag force exerted on the supporting legs in the jumping process, indicating that the drag force varies linearly with height $h$. The drag force will reduce to zero once the supporting legs completely leave the water surface. We also compared the results with those of the original nickel foam sheets with the same size. Although the drag force of the original nickel foam is slightly greater (ca. −9.3 N) than that of the supporting legs (−9.0 N), the former needs to jump at a height ($h$ = ∼5.3 mm) about 9 times that of the latter ($h$ = ∼0.6 mm) in order to entirely leave the water surface. This result means that much more energy (ca. 24.6 mJ) is consumed for the original nickel foam sheets compared to the supporting legs (ca. 2.7 mJ) in the jumping process. Figure 5b illustrates the influence of the CA on the maximum drag force, leaving height, and energy consumption of the supporting legs in the process of jumping. This shows that high CA results in not only a smaller drag force exerted on the supporting legs but also a lower leaving height and energy consumption. Therefore, the superhydrophobic property of the supporting legs is greatly beneficial for the robot leaving the water surface in the process of jumping.

**5. Numerical Analysis on the Falling Process.** In order to stand stably on water after falling, the descent velocity of the microrobot must reduce to zero before the supporting legs penetrate the water surface. As mentioned above, the descent velocity of the robot is up to 1.6 m $s^{-1}$ as it reaches the water surface. Then the descent velocity reduces quickly because of increasing upward force in the falling process. On the basis of eq 2, the falling process of the robot on the water surface can be described by the numerical model

$$m\ddot{h} - \frac{1}{2}S\rho\dot{h}^2 + \rho ghS - \gamma L\sin\phi + mg = 0 \qquad (6)$$

where $m$ is the mass of the robot. Considering $\dot{h}(0)$ = 1.6 m $s^{-1}$ and $h(0)$ = 0, variation of the descent velocity is calculated according to eqs 2 and 6, as shown in Figure 6. The robot stops

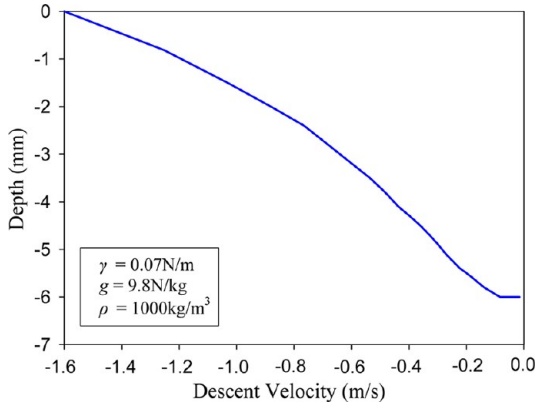


**Figure 6.** Variation of the descent velocity as the microrobot falls on the water surface.

falling at a depth ($h$) of −6.0 mm (corresponding to an upward force of 0.42 N), smaller than the maximal immersion depth (i.e., $h$ = −7.0 mm) calculated for the supporting legs (corresponding to an upward force of 0.48 N; see the Supporting Information, Figure S3), implying that the microrobot is able to stand stably on the water surface after falling. We also revealed that an increase in the CA not only raises the upward force of the supporting legs but also enables them to

immerse deeper beneath the water surface without sinking (see the Supporting Information, Figure S4).

On the basis of the above analyses, we demonstrate that the superhydrophobicity of the supporting legs is crucial for the jumping capability of the microrobot because it not only increases the upward force of the supporting legs but also reduces the energy consumption in the jumping process, which ensures that the robot jumps freely and continuously on water. Although the speed and agility of the robot are not comparable to those of a real water strider,[13] the present results still offer possibilities of fabricating a water-jumping microrobot by utilizing superhydrophobic nickel foam sheets as supporting and actuating legs.

## CONCLUSIONS

In summary, a bioinspired microrobot capable of jumping on the water surface like a real water strider was fabricated in this study. Despite the fact that the microrobot was much larger and heavier than about 1100 water striders, it was still able to continuously jump on the water surface without sinking. Numerical modes were established to investigate the factors affecting the jumping mechanism of the robot. Experimental results and theoretical simulations demonstrated that the superhydrophobicity of the supporting legs not only increased their upward force but also reduced their energy consumption in the process of jumping, providing alternative applications of porous and superhydrophobic materials in advanced robotic systems. Although previous microrobots mimicked the horizontal skating motions of aquatic insects,[3,6,17−20] the continuously jumping characteristics of a bioinspired microrobot on the water surface were reported here for the first time. Therefore, the findings of the present study yield valuable insights into fabricating highly agile bioinspired microrobots that have wide potential applications in aquatic environmental control, water pollution monitoring, and the like.

## ASSOCIATED CONTENT

### Supporting Information

Effect of the $Cu_2(OH)_2CO_3$ concentration on the morphology of the as-prepared nickel foam, mechanical stability of the superhydrophobic coatings on the nickel foam, movie of the microrobot jumping on the water surface, calculation of the maximal immersion depth of the supporting legs, effect of the CA on the maximal immersion depth and upward force of the supporting legs, and calculation of the Reynolds number (*Re*). This material is available free of charge via the Internet at http://pubs.acs.org.

## AUTHOR INFORMATION

### Corresponding Author

*E-mail: panqm@hit.edu.cn.

### Author Contributions

‡These authors contributed equally to the work.

### Notes

The authors declare no competing financial interest.

## ACKNOWLEDGMENTS

This work was financially supported by a self-planned task of the State Key Laboratory of Robotics and System of Harbin Institute of Technology (Grant SKLRS200901C) and the National Natural Science Foundation of China (Grant 50803013).

## REFERENCES

(1) Bush, J. W. M.; Hu, D. L. *Ann. Rev. Fluid Mech.* **2006**, *38*, 339−369.
(2) Hu, D. L.; Chan, B.; Bush, J. W. M. *Nature* **2003**, *424*, 663−666.
(3) Suhr, S. H.; Song, Y. S.; Lee, S. J.; Sitti, M. *Proc. Rob. Sci. Syst. I* **2005**, 319−325.
(4) Takonobu, H.; Kodaira, K.; Takeda, H. *IEEE/RSJ International Conference on Intelligent Robots and Systems*, Edmonton, Alberta, Canada, 2005;IEEE: Piscataway, NJ, 2005; pp 1754−1759.
(5) Song, Y. S.; Sitti, M. *IEEE International Conference on Robotics and Automation*, Rome, Italy, 2007; IEEE: Piscataway, NJ, 2007; pp 980−984.
(6) Zhang, X. B.; Zhao, J.; Zhu, Q.; Chen, N.; Zhang, M. W.; Pan, Q. M. *ACS Appl. Mater. Interfaces* **2011**, *3*, 2630−2636.
(7) Shin, B.; Kim, H.Y.; Cho, K. J. *Proceedings of the 2nd Biennial IEEE/RAS−EMBB International Conference on Biomedical Robotics and Biomechatronics*, Scottsdale, AZ, 2008; IEEE: Piscataway, NJ, 2008; pp 127−135.
(8) Chung, S. K.; Ryu, K.; Cho, S. K. *The 22nd International Conference on Micro Electro Mechanical Systems (MEMS 2009)*, Sorrento, Italy, 2009; 2009, 1083−1086.
(9) Gao, T. H.; Cao, J. Y.; Zhu, D. Y.; Zhi, J. Z. *Proc. IEEE Int. Conf. Integr. Technol.* **2007**, 685−690.
(10) Wu, L. C.; Sun, F. C.; Yuan, H. B. *Robot* **2010**, *32*, 443−448.
(11) Gao, T. H.; Zhu, D. Y.; Cao, J. Y.; Qin, Y. X. *IEEE Int. Conf. Rob. Biomimetics* **2007**, *1*−*5*, 775−780.
(12) Hu, D. L.; Chan, B.; Bush., J. W. M. *Elsevier Sci.* **2005**, *6*, 256−263.
(13) Gao, X.; Jiang, L. *Nature* **2004**, *432*, 36.
(14) Feng, X. Q.; Gao, X. F.; Wu, Z. N.; Jiang, L.; Zheng, Q. S. *Langmuir* **2007**, *23*, 4892−4896.
(15) Shi, F.; Niu, J.; Liu, J.; Liu, F.; Wang, Z.; Feng, X.; Zhang, X. *Adv. Mater.* **2007**, *19*, 2257−2261.
(16) Jiang, L.; Yao, X.; Li, H.; Fu, Y.; Chen, L.; Meng, Q.; Hu, W.; Jiang, L. *Adv. Mater.* **2010**, *22*, 376−379.
(17) Floyd, S.; Sitti, M. *IEEE Trans. Rob.* **2008**, *24* (3), 698−709.
(18) Floyd, S.; Keegan, T.; Sitti, M. *Proceedings of the IEEE/RSJ Intelligent Robot Systems Conference*, Beijing, China, 2006; IEEE: Piscataway, NJ, 2006; pp 5430−5436.
(19) Suzuki, K.; Takanobu, H.; Noya, K.; Koike, H.; Miura, H. *Proceedings of the IEEE/RSJ International Conference on Intelligent Robots and Systems (IROS07)*, San Diego, CA, 2007; IEEE: Piscataway, NJ, 2007; pp 590−595.
(20) Ozcan, O.; Wang, H.; Taylor, J. D.; Sitti, M. *2010 IEEE International Conference on Robotics and Automation*, Anchorage, AK, 2010; IEEE: Piscataway, NJ, 2010; pp 3799−3804.
(21) Lee, D. G.; Kim, H. Y. *Langmuir* **2008**, *24*, 142−145.
(22) Pan, Q. M.; Wang, M. *ACS Appl. Mater. Interfaces* **2009**, *1*, 420−424.
(23) Keller, J. B. *Phys. Fluids* **1998**, *10*, 3009−3010.
(24) Song, Y. S.; Sitti, M. *IEEE Trans. Rob.* **2007**, *23* (3), 578−589.
(25) Song, Y. S.; Suhr, H.; Sitti, M. *Proceedings of the IEEE International Conference on Robotics and Automation*, Orlando, FL, 2006; IEEE: Piscataway, NJ, 2006; pp 2303−2310.
(26) Pan, Q. M.; Liu, J.; Zhu, Q. *ACS Appl. Mater. Interfaces* **2010**, *2*, 2026−2030.